Structural, electronic and hyperfine characterization of pure and Ta-doped $ZrSiO_4$

R. E. Alonso,[1,3] L. Errico,[2,3] M. Taylor,[1,3] A. Svane,[4] and N. E. Christensen[4]

[1]*Departamento de Ciencias Básicas, Facultad de Ingeniería, UNLP, Calle 48 y 115 S/N, La Plata, CP 1900, Argentina*

[2]*Universidad Nacional del Noroeste de la Pcia. de Buenos Aires (UNNOBA), Monteagudo 2772, Pergamino, CP 2700, Buenos Aires, Argentina*

[3]*Instituto de Física La Plata-CCT La Plata, CONICET. CC 67, CP 1900 La Plata, Argentina*

[4]*Department of Physics and Astronomy, Aarhus University, DK-8000 Aarhus C, Denmark*

(Received 28 October 2014; revised manuscript received 9 January 2015; published 27 February 2015)

The electronic structure of pure and Ta-doped $ZrSiO_4$ in the tetragonal $I4_1/amd$ phase with and without defects has been studied using the *ab initio* full-potential linear augmented plane wave plus local orbitals method. From the determined charge densities, the electric field gradient tensor at native Zr sites and at Ta impurities localized on cation sites of $ZrSiO_4$ were derived and compared to experimental data obtained using hyperfine techniques. The effects of the Ta probe atom, including its different charge states on the lattice, are investigated. In addition, different types of defects, such as O or Si vacancies, Ta replacing Si, and Ta enclosed in microstructures of SiO_2 phases, are examined. The combination of experiments and theory enables us to identify the different interactions observed in Ta-doped $ZrSiO_4$ and to elucidate the role played by different defects.

DOI: 10.1103/PhysRevB.91.085129 PACS number(s): 71.15.−m, 76.80.+y, 71.15.Mb, 71.20.Nr

I. INTRODUCTION

Zircon ($ZrSiO_4$) is a common accessory mineral in igneous and metamorphic rocks [1]. It has attracted the interest of researchers because it can be used as raw material for a large number of applications. Its chemical stability makes zircon suitable for environmental barrier coatings in the chemical industry. For the same reason, it has been considered in the nuclear industry for high level waste disposal of actinides [2]. On the other hand, it possesses a high dielectric constant and a large energy gap, thus emerging as a high-κ gate dielectric material in the metaloxide-semiconductor technology [3]. Zircon also has a high refraction index, a light color compatibility with ceramic colors, and a low solubility in glass. These features make it the dominant opacifier for glasses [4].

Natural zircon is characterized by some kind of amorphization as a result of the accumulation of radiation damage over time, due to radioactive Th, Pu, and U nuclei commonly present as impurities [5]. In the process, α-recoil nuclei directly amorphize nanometric volumes of the structure, whereas an increase of the unit-cell volume was observed in the nearby still-periodic structure [6]. As a consequence of the radiation damage, crystalline and amorphous domains coexist at a submicrometric scale and can be observed, for example, by transmission electron microscopy [7].

The ^{91}Zr nuclear magnetic resonance (NMR) and the time differential perturbed angular correlation (TDPAC) using $(^{181}\text{Hf} \rightarrow)^{181}\text{Ta}$ as probe techniques are highly efficient in investigating zirconium-containing compounds at the nanoscopic scale. Both techniques provide information about the hyperfine interaction between the probe nucleus and its surroundings, and thereby the charge distribution in the close vicinity of the probe can be analyzed. These techniques are efficient for the analysis of local disorder, and, in the case of zircon, they are powerful tools for studying the impact on the structure of the radiation damage [8]. In the reported ^{91}Zr-NMR experiments [9], a well-defined nuclear quadrupole interaction (NQI) has been found, which was assigned to the regular Zr site in zircon. In the case of the $(^{181}\text{Hf} \rightarrow)^{181}\text{Ta}$ TDPAC experiments, the results are more complicated because multiple hyperfine interactions were reported. In this situation the interpretation of the various electric field gradient (EFG) fractions (measured at an impurity site) is by no means straightforward. One of the NQI (observed in all the experiments independently of the nature, origin, or history of the sample) was associated with Ta probes at the Zr sites, but discrepancies with respect to the hyperfine parameters that characterize this NQI persist. The other observed NQIs were not identified [10–13].

In the present paper, an *ab initio* study of pure and Ta-doped $ZrSiO_4$ is performed in order to understand the available experimental TDPAC and NMR results. We analyze different charge states that can be assigned to the Ta impurity probe. We also consider the local polarization effects that can be induced by an extra unpaired electron on Ta. Further issues addressed are the possibility that Ta occupies a Si site instead of a Zr site, the influence of O or Si vacancies, and the possibility that the probe $(^{181}\text{Hf} \rightarrow)^{181}\text{Ta}$ is incorporated in a spurious SiO_2 phase formed within the zircon host. The doped structures are optimized using force calculations, relaxing all the atomic positions in order to take into account the structural distortions of the lattice caused by the impurity-probe atoms. From the self-consistent potentials, the hyperfine parameters at the Zr and Ta sites are derived, and finally the results are compared to experimental results reported in the literature.

The paper is organized as follows. In Sec. II, the calculational method is presented. In Sec. III, we analyze pure zircon in order to compare it with experimental NMR results and to test the validity of the approach. In this section we also discuss the energy gap of pure zircon. Section IV presents the study of Ta-doped zircon assuming that Ta is an impurity that replaces Zr. The effect of the charge state of Ta on the EFG and the local magnetic moment on this site is also examined. In Sec. V, we consider different possible defect structures involving Ta, which may be present in the samples investigated by experiments. In Sec. VI, the calculated EFGs for the different situations are compared with the available

experimental results, and, finally, Sec. VII gives a summary and conclusions.

II. METHOD OF CALCULATION

The crystal structure of zircon ($ZrSiO_4$) resembles that of garnet and comprises an arrangement of SiO_4 tetrahedra and ZrO_8 dodecahedra [14]. Two different phases of $ZrSiO_4$ exist depending on pressure, corresponding to two different arrangements of these polyhedra. In the low-pressure phase, the Bravais lattice is tetragonal body-centered with 12 atoms in the unit cell. The space group is $I4_1/amd$ (D_{4h}^{19}, no. 141). The structure is characterized by the lattice parameters $a = 6.6039$ Å and $c = 5.9783$ Å and two internal parameters y and z that determine the positions of the oxygen atoms ($y = 0.06586$ and $z = 0.19533$) [15]. The structure has only one crystallographic Zr site, coordinated to eight oxygen atoms (ONN). Four of these ONN are located at 2.13 Å from the Zr site (ONN1), while the other four are located at 2.27 Å (ONN2).

The EFG tensor is a traceless symmetric tensor of rank two whose components, denoted by $V_{i,j}$, are defined by the second derivative (with respect to the spatial coordinates x_i) of the Coulomb potential $V(\mathbf{r})$ created by the charge density surrounding a given nucleus [16], for simplicity located at the origin of coordinates

$$V_{i,j}\,(\vec{r}=0) = \left.\frac{\partial^2 V}{\partial x_i \partial x_j}\right|_{\vec{r}=0}. \tag{1}$$

The EFG can be determined once the total charge distribution has been accurately calculated (for details of the calculation of the EFG see Ref. [17]). The eigenvalues of the EFG tensor are denoted V_{XX},V_{YY}, and V_{ZZ}, and the conventional choice is $|V_{XX}| \leqslant |V_{YY}| < |V_{ZZ}|$. Hence, V_{ZZ} is the largest eigenvalue of the EFG tensor, and the asymmetry parameter η is a measure of the difference between the two eigenvalues V_{XX} and V_{YY}

$$\eta = \frac{V_{XX} - V_{YY}}{V_{ZZ}}. \tag{2}$$

V_{ZZ} is related to the experimentally determined nuclear coupling constant frequency ν_Q through [16]

$$\nu_Q = \frac{eQV_{ZZ}}{h}. \tag{3}$$

In this equation, Q denotes the largest component of the nuclear quadrupole moment tensor of the sensitive TDPAC/NMR states $Q(^{181}\mathrm{Ta}) = 2.26_5 b$ [18] and $Q(^{91}\mathrm{Zr}) = -0.206b$ [19] for TDPAC and NMR probes, e is the electron charge, and h denotes Planck's constant.

In order to determine the self-consistent potential and the charge density inside the pure and Ta-doped zircon cells, *ab initio* calculations were performed using the full-potential linear augmented plane wave plus local orbital [(L)APW+lo] method in a scalar relativistic version [20], as implemented in the WIEN2K code [21]. From these results, the EFG tensor at the Zr nucleus in the pure system and at the Ta and Zr nucleus in the doped structure (Ta impurity replacing Zr) were determined, in the last case, taking properly into account the structural and electronic effects introduced by the impurity in the host lattice. For all calculations, we used the experimental lattice parameters [15].

For the simulation of the diluted Ta impurity, the supercell (SC) scheme was employed following the general guidelines reported in Ref. [22]. Calculations were made for a periodic arrangement of eight unit cells of $ZrSiO_4$. The resulting 192-atom SC (the body-centered symmetry is lost when the impurity is introduced) has dimensions $a^* = 2a = b^* = 2b = 13.2078$ Å and $c^* = 2c = 11.9566$ Å. Then, one of the Zr atoms was replaced by a Ta atom. This corresponds to an ordered $Zr_{31}TaSi_{32}O_{128}$ compound (about 3 at. % doping). Although this Ta concentration is large compared with the parts per million (ppm) dilution in the samples used in the TDPAC experiments, the choice of the 192-atom SC keeps the Ta atoms sufficiently far from each other (at least 11.30 Å) to avoid significant interactions between impurities. The muffin-tin radii used were 1.06 Å for Ta and Zr and 0.80 Å for Si and O. These values were selected as a compromise between the computational times and the possibility of minimizing energy by varying the atomic positions. In order to get the equilibrium structures, once self-consistency was achieved, quantum-mechanically derived forces on the ions were obtained, the ions were displaced according to a Newton-damped scheme, and then the relaxed positions of the atoms were obtained. This procedure was repeated until the forces on the ions were below a tolerance value of 0.01 eV/Å [22].

Zirconium is characterized by a strong overlap of the semicore $4s$ and $4p$ states with the valence $4d$ wave functions [23]. Therefore, the Zr-$4s$ and $4p$ were included as valence states. Similarly, the Ta semicore $5s$, $5p$, and $4f$ states were included in the self-consistent description. To improve linearization, local orbitals for Zr-p and s; Ta-s, p, and f; and O-s states were added [21]. The energy cutoff criterion was $R_{mt}K_{\max} = 7$ for the pure $ZrSiO_4$ system (R_{mt} denotes the smallest muffin-tin radius and $K_{\max}$ the largest wave number of the basis set). Integration in reciprocal space was performed using the tetrahedron method [24], considering 300 k-points in the full Brillouin zone (BZ), which are reduced to 10 k-points in the irreducible wedge of the BZ (IBZ). In the case of the doped system, the inclusion of an isolated Ta impurity in the $ZrSiO_4$ host was analyzed by building a 192-atom SC. With this large cell, the calculations turned out to be computationally highly demanding; therefore, the $R_{mt}K_{\max}$ value and the number of k-points must be carefully optimized. We have performed several tests in the large cell, including those corresponding to the metallic states produced by the Ta-impurity atom. For $R_{mt}K_{\max} = 6$ and up to 100 k-points in the BZ (six k-points in the IBZ), the EFG values are converged to a precision of 0.2×10^{21} V/m^2, which is of the same order of accuracy as the experimental results. Bond lengths and energy differences can be obtained with similar accuracy. We have also tested at the beginning of the calculations the convergence of all the significant parameters (energy differences, forces, bond lengths, and magnetic moments). In order to plot the density of states (DOS), we calculate eigenvalues at a denser mesh of 1000 k-points in the BZ.

For the exchange correlation (XC) potentials, we used the local spin-density approximation (LSDA, Ref. [25]) and the Perdew-Burke-Ernzerhof (PBE) parameterization of the generalized gradient approximation (GGA) for solids

TABLE I. Comparison of experimental and calculated oxygen coordinates and V_{ZZ} values for pure $ZrSiO_4$. $Q = -0.176b$ (Ref. [27]) was used to calculate V_{ZZ} from the experimentally determined nuclear coupling constant frequency ν_Q (20.47 MHz, Ref. [9]). In all cases, $\eta = 0$.

	y	z	V_{ZZ} at Zr site [10^{21} V/m^2]	V_{ZZ} at Si site [10^{21} V/m^2]
Experiment	0.06586[a]	0.19533[a]	4.83	–
GGA-PBE experimental structure	0.06586	0.19533	5.3	−2.0
LDA experimental structure	0.06586	0.19533	5.5	−2.0
GGA-PBE predicted structure	0.0657	0.193	5.1	−2.4
LDA predicted structure	0.0661	0.193	5.1	−2.1

[a]Data from Ref. [15].

(GGA-PBE) [26]. The local density approximation (LDA) and GGA-PBE produce only small differences, so, in the following only GGA-PBE results will be presented.

III. PURE $ZrSiO_4$

As a first step and in order to evaluate the accuracy of the method as well as the different XC potentials utilized to describe the system, several calculated properties of the pure $ZrSiO_4$ compound will be compared to the experimental results. As mentioned, zircon was characterized using ^{91}Zr-NMR, and the EFG at the Zr site was determined. Bastow [9] measured the nuclear quadrupole frequency ν_Q at the Zr sites in $ZrSiO_4$ at room temperature by means of magic angle spinning (MAS) NMR (MAS-NMR). The reported value for ν_Q was 20.47 MHz. In agreement with the symmetry of the structure, $\eta = 0$ was found. Using Eq. (3) and the value $Q(^{91}\text{Zr}) = -0.206b$ for the nuclear quadrupole moment of ^{91}Zr (derived by atomic beam resonance methods [19]), the EFG obtained at the Zr site is $V_{ZZ} = 4.13\,10^{21}$ V/m^2. More recent papers found a lower value for the nuclear quadrupole moment of the MAS-NMR sensitive state of ^{91}Zr, $Q(^{91}\text{Zr}) = -0.176b$ [27], which leads to $V_{ZZ} = 4.83\,10^{21}$ V/m^2.

Table I presents the calculated results for the EFG at the Zr and Si sites in pure $ZrSiO_4$, considering the experimental lattice and positional parameters and using the LDA and GGA-PBE approximations. In addition, the experimental results obtained by Bastow [9] are included. Only the EFG on the Zr site, where experimental data are available, will be analyzed. The asymmetry parameter η is zero due to the cell symmetry. At the experimental oxygen coordinates, LDA predicts a value of V_{ZZ}, which is about 4% larger than that obtained using GGA-PBE. The LDA and GGA-PBE calculations performed using the experimental lattice parameters and atomic positions predict forces of about 0.6 eV/Å on the O atoms and close to zero for Zr and Si. Thus, total force minimization was performed to optimize the atomic positions of the oxygen atoms. The internal position parameters y and z predicted by both XC models are in excellent agreement with the experimental values (see Table I). Analyzing the predicted equilibrium structures, the major displacement from the experimental positions is along the z direction, which leads to a shortening of the Zr-O distance from 2.128 Å to 2.127 Å (2.124 Å) using LDA (GGA-PBE) and an increase of the Si-O distance from 1.623 Å to 1.630 (1.633 Å) for the LDA (GGA-PBE) cases. For both XC approximations, the corresponding calculated V_{ZZ} values at the Zr site are smaller than those obtained with the experimental internal coordinates. Compared to the experimental results, the calculated EFG is 5–6% larger than the value obtained using the most recent determination of the ^{91}Zr nuclear quadrupole moment.

In Fig. 1, we present the total DOS and the partial DOS (PDOS) of each of the constituent atoms obtained with the LDA calculations (very similar results were obtained using the GGA-PBE approximation, so they are not shown). The valence band of zircon is dominated by the O-2p states; however, there is a considerable contribution of Si-3s and 3p states (and, to a lesser extent, Zr-4d). These hybridization contributions evidence the covalent admixture of the Si–O bonds. Above the Fermi level, the conduction band has predominantly Zr-4d character, an indication of the ionic nature of the Zr-O bonds. These conclusions about the nature of the Zr-O and Si-O bonds are also visible in Fig. 2, where the electron density is plotted

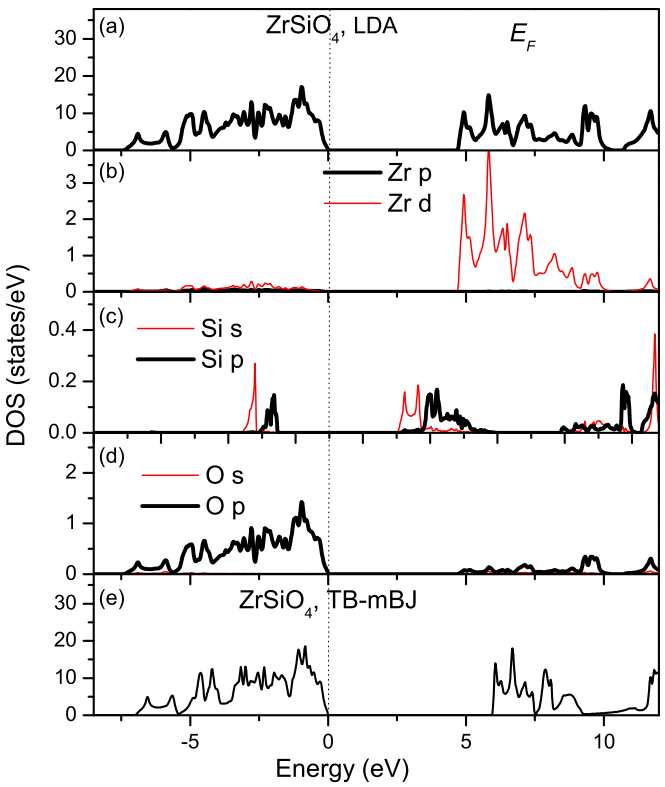

FIG. 1. (Color online) Total and partial DOS of the dominant angular character of the constituent atoms in $ZrSiO_4$. Energies are referred to the Fermi level (E_F), denoted as a vertical dotted line. (a)–(d) Results obtained using LDA. (e) The total DOS as obtained with the TB-mBJ functional.

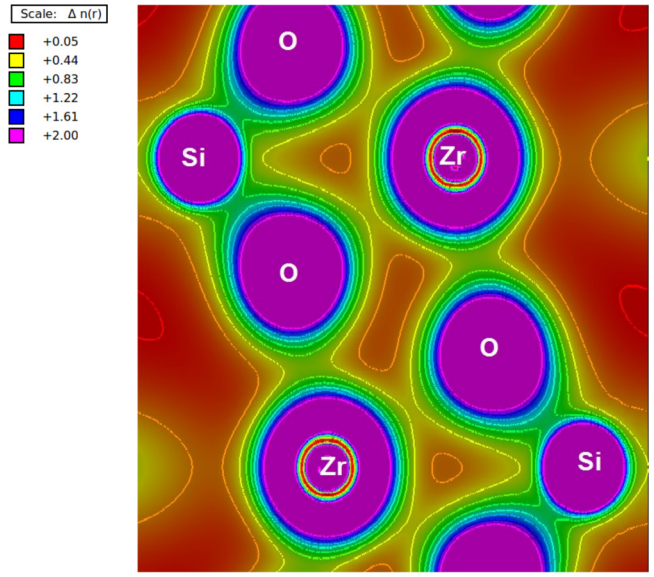

FIG. 2. (Color online) Electron density plot of in $ZrSiO_4$ in the yz plane with the origin at (1/2, 0, 0).

in a plane parallel to the yz plane with the origin at (1/2, 0, 0) of the body-centered unit cell. This plane was selected because it contains the three specimens and at least two of the first nearest neighbors of the Zr and Si atoms. The green contour, corresponding to electron density 0.83 e/Å^3, is shared between the Si atom and its O nearest neighbors while it forms a closed curve around the Zr atom, i.e., a slight tendency to bond formation between Si and O is seen.

Both LDA and GGA-PBE calculations predict the correct semiconducting nature of zircon with a band gap of 4.7 eV between the valence and conduction bands. Different spectroscopic papers reported that the band gap of zircon lies in the ultraviolet region in the range 230–280 nm (4.42–5.38 eV) [28]. Kawamoto *et al.* [29] performed calculations using the LDA parameterized by Perdew and Zunger [30] and obtained a band gap of 4.58 eV, in good agreement with the present value. Based on the well-known underestimation of semiconductor band gaps in the LDA and GGA-PBE calculations, Kawamoto *et al.* [29] included an empirical factor for the estimation of the gap of the system. This factor was obtained by simultaneously correcting the calculated gaps of SiO_2 and ZrO_2 to fit the experimental data. Assuming that the same empirical factor can be applied to silicates across a range of Zr concentrations, they obtain a gap of 7.59 eV for $ZrSiO_4$, a value 40% larger than the experimental band gap. In the present paper, to avoid the use of empirical factors and extra hypotheses, we utilized the Tran-Blaha modified Becke-Johnson (TB-mBJ) [31] approximation for the XC potential to explore the band gap correction. This leads to a band gap of 5.90 eV. This result is in very good agreement with the experimental ones [28]. In Figs. 1(a) and 1(e), the total DOS obtained using the LDA and TB-mBJ approximations are compared. The Zr-d states (conduction band) are shifted to higher energies by around 1.25 eV, accounting for the gap increase, but the TB-mBJ approximation does not simply lead to a rigid-band shift behavior: While the conduction Zr-d states are moved to higher energies, the O-2s bands are moved down by about 2.0 eV, but the deep Zr-4p states remain unchanged.

IV. THE Zr(Ta)SiO_4 SYSTEM

To perform a TDPAC experiment, a probe atom must be introduced in the system under study. Since Zr naturally contains Hf impurities, Zr compounds inevitably contain Hf atoms substituting for Zr atoms. Hence, the (^{181}Hf $\rightarrow$)^{181}Ta probes can easily be incorporated in the system by neutron irradiation. The substitution of a native Zr atom by the Ta impurity probe does not produce significant changes on the bulk properties of the material due to their very low concentration (as low as a few ppm). Nevertheless, the local symmetry and the electronic structure in the vicinity of the probe site could be significantly altered from that of the native atom. Since the TDPAC technique measures the EFG at the impurity probe site, its magnitude may be very sensitive to fine details of the symmetry of the charge distributions in the close vicinity (at the subnanoscopic scale) of the probe. The structural, electronic, and even spin-polarization effects (as recently shown in Refs. [32] and [33]) induced by the probe could have a strong influence on the measured EFG. Therefore, the EFG could be, in principle, very different from that for the unperturbed host lattice sites. Not long ago, very simplistic models were frequently applied to calculate the EFG in many materials, and the obtained values were correlated with the experimental results [34]. These simple models dramatically failed to correctly predict the EFG in many compounds due to the fact that they do not take properly into account the impurity character of the TDPAC probes. In the following, we analyze one by one the effects of different electronic and structural variables on the EFG.

In the first calculation, the self-consistent electronic structure of the 192-atom SC with all atoms in their initial unrelaxed positions was calculated. In an ideal ionic model, the valence of Ta is 5+. When a Ta atom replaces a Zr^{+4} atom in the SC, there is one electron in excess located at a donor impurity level. The DOS of Ta-doped $ZrSiO_4$ shown in Fig. 3(a) (left panel) confirms this simple picture: The Ta impurity induces a partially filled impurity band at the bottom of the conduction band, and the resulting system is metallic. The states located at the Fermi energy (E_F) correspond to states that are spatially located at Ta and their ONN atoms and have Ta-d character (see Fig. 4), thus resembling a Ta acting with valence +4. Based on this, we name this charge state as Ta^{+4}. It may be observed that only one of the Ta-d components is partially occupied while the others remain unfilled. [For this selection of the Zr-substituted atom at (0,0,0), it is d_{xz}. In the real space, the lobes of the d_{xy} orbital point into the interstitial region]. Note that the Ta impurity band is described as a very sharp peak, indicating that interaction between Ta orbitals is small for this SC size.

Comparing the EFG at the Zr and Ta sites in pure and Ta-doped $ZrSiO_4$ (Table II), it is seen that V_{ZZ} changes from 5.3×10^{21} V/m^2 (Zr site) to 35.7×10^{21} V/m^2 (Ta^{+4} site) before taking into account any effect of the rearrangement of the atoms of the host structure. In order to evaluate the spatial extent of the impurity effects and also to check the convergence

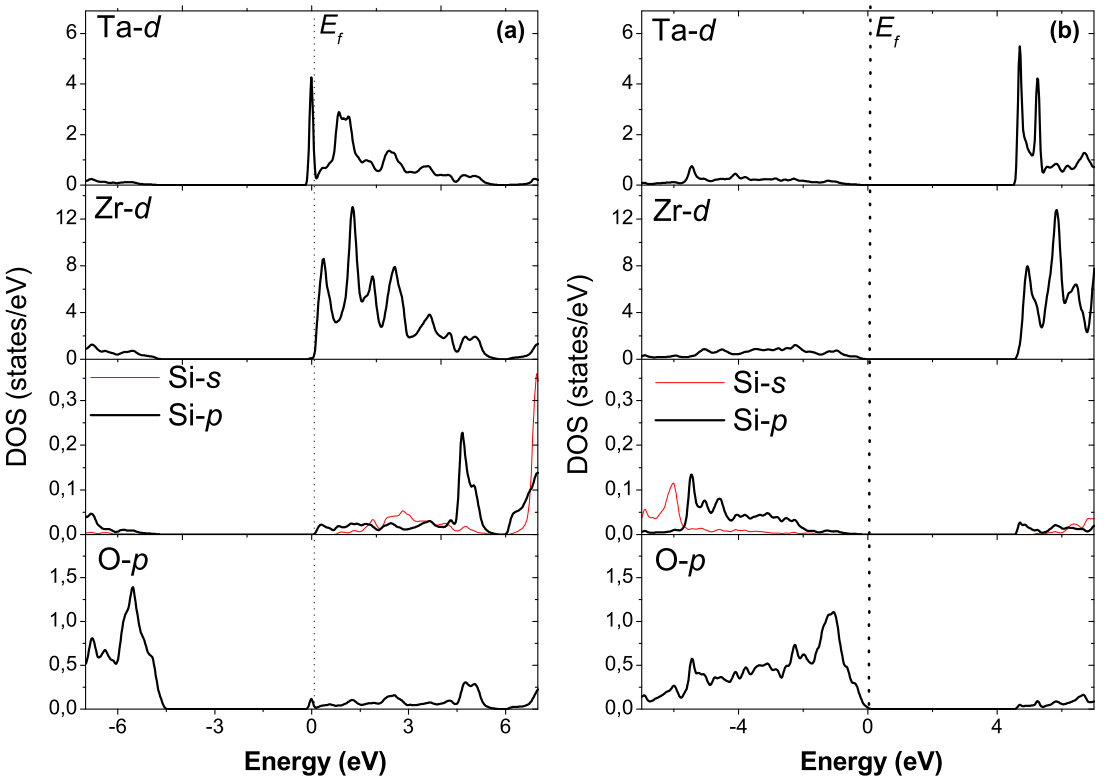

FIG. 3. (Color online) PDOS of Ta-doped $ZrSiO_4$ for the Ta^{+4} (a) and Ta^{+5} (b) charge states. Energies are referred to as the Fermi level (E_F), which is denoted by vertical dotted lines. In both cases, Ta replaces a Zr.

of the SC dimension, Table II includes the corresponding V_{ZZ} values for the nearest Si and Zr neighbors of the Ta impurity, which are at a distances of 2.99 Å and 3.62 Å from Ta, respectively, in the unrelaxed structure (referred to as ZrI and SiI in the following) together with the V_{ZZ} corresponding to Zr and Si atoms farther away from Ta [SiII and ZrII, at distances of 7.59 Å (Zr) and 8.64 Å (Si) from Ta]. Due to the large Ta-ZrII/SiII separation, the perturbation induced by the impurity at these sites should be negligible, and their electronic structure should resemble that of the pure $ZrSiO_4$ system. Indeed, comparing the calculated V_{ZZ} in Table I (GGA-PBE calculation) and II, the ZrI and SiI atoms are seen to have V_{ZZ} values relatively close to those of the unperturbed ones (Zr and Si in pure $ZrSiO_4$) but with η in the order of 0.10, while the more distant ZrII and SiII atoms have the same hyperfine parameters as those obtained for the pure $ZrSiO_4$ system. This result is important as a check of the overall effects of the SC model employed in this work.

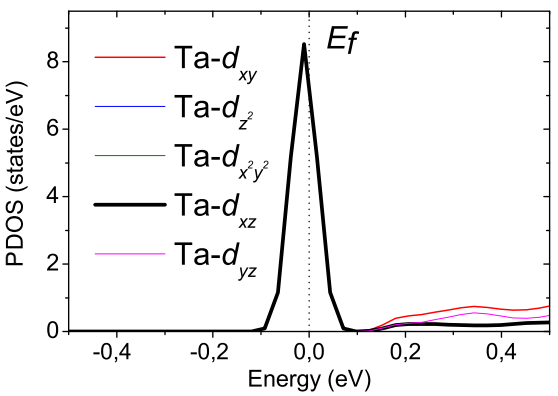

FIG. 4. (Color online) Orbital-resolved PDOS of Ta d states in the Fermi level energy region. The calculations correspond to the spin-polarized calculations and the charge state Ta^0.

A second step in the analysis is to relax the atomic positions within the SC. The substitution of Zr by Ta impurity introduces local distortions in the host. The structural relaxation leads to a contraction of the eight Ta-ONN bond lengths: the Ta-ONN1 bond lengths are shortened by about 0.03 Å, while the Ta-ONN2 bond lengths are reduced by 0.08 Å (see Table III). This contraction of the Ta-ONN bond lengths is to be expected since Ta has a smaller atomic radius than Zr. As has been observed for other compounds [32,33], it seems that Ta seeks to reconstruct its local neighborhood in tantalum oxide (TaO_2), in which the Ta-O bond lengths are around 2.02 Å. The magnitude of the atomic distortions decreases rapidly when going from the nearest oxygen neighbors to other shells (not shown). Concerning the EFG at the Ta^{+4} site, the effect of the structural relaxation is to reduce the V_{ZZ} value from 35.7 to 27.0×10^{21} V/m^2 (Table II). Concerning the ZrI and SiI, the EFG tensor at these sites is sensitive to the relaxation of the Ta-ONN: The asymmetry increases to 0.18 and 0.39 for ZrI and SiI, respectively. For the more distant Zr and Si atoms (ZrII and SiII), the asymmetry and V_{ZZ} recover the values of the pure system, thus indicating that the effect of the Ta impurity is negligible beyond the nearest neighbor atomic shells.

Going back to the effect of the substitution of Zr^{+4} by Ta on the electronic structure of the impurity-host system, it has been theoretically predicted (and confirmed by reanalyzing the TDPAC data) that for Ta-doped ZrO_2 and HfO_2, the extra d

TABLE II. Calculated EFGs using GGA-PBE on the atomic sites in the $Zr_{31}TaSi_{32}O_{128}$ SC in units of 10^{21} V/m^2. Two Ta charge states are considered, and the values with and without atomic relaxations are quoted. For the Ta^{+4} charge state, a spin-polarized solution was also found (last column). ZrI, SiI and ZrII, SiII denotes Ta first and second Zr and Si neighbors, respectively.

	Ta^{+4} Unrelaxed	Ta^{+4} Relaxed	Ta^{+5} Unrelaxed	Ta^{+5} Relaxed	Ta^{+4} Relaxed, spin-polarized
Site	V_{ZZ}/η	V_{ZZ}/η	V_{ZZ}/η	V_{ZZ}/η	V_{ZZ}/η
Ta	35.7/0.00	27.0/0.00	10.4/0.00	12.6/0.00	29.7/0.00
ZrI	5.4/0.11	5.3/0.18	5.5/0.37	6.1/0.50	5.3/0.14
ZrII	5.3/0.00	5.4/0.05	5.2/0.06	5.3/0.06	5.3/0.02
SiI	−2.0/0.13	−2.4/0.39	−2.0/0.49	−2.5/0.66	−2.4/0.34
SiII	−2.0/0.00	−2.0/0.01	−1.9/0.00	−2.0/0.02	−2.0/0.01

electron that populates the donor impurity level may be removed in some way from the impurity neighborhood, thus leaving the impurity acting (in the framework of an ionic model) as Ta^{+5} [32,33]. To apply the same idea to $Zr(Ta)SiO_4$, one electron was removed from the SC. In order to maintain the neutrality of the cell, a homogeneous negative background was added to the whole cell. We will denote this charge state "Ta^{+5}." For this charge state, the impurity level at E_F (partially occupied in the case of Ta^{+4}) becomes empty, and the system recovers the semiconducting character of $ZrSiO_4$ (see Fig. 3, right panel). The effect of the change in the charge state in the EFG tensor is a drastic reduction of the magnitude of V_{ZZ}. As can be seen in Table II, V_{ZZ} changes from 35.7×10^{21} V/m^2 (Ta^{+4}, unrelaxed structure) to 10.4×10^{21} V/m^2 (Ta^{+5}, unrelaxed structure). Comparing the calculations for the two charge states for the same (unrelaxed) structure, the change in the EFG going from Ta^{+4} to Ta^{+5} is solely caused by the depopulation of the donor impurity level introduced by Ta, i.e., by the change of symmetry of the electronic charge in the close vicinity of Ta. Additionally, for Ta^{+5} an increment in the η parameter at SiI and ZrI sites is observed (see Table III).

The effect of the relaxation of the atomic positions in the cell for the Ta^{+5} charge state may be seen in Table III (fourth column). The contraction of the Ta-ONN bond is larger in this case compared with the previous calculations for the Ta^{4+} case. This is due to the change in the Coulomb interaction. The predicted Ta-ONN distances are in quite good agreement with those calculated considering the empirical ionic radii [35] for the different Ta and O coordination in the zircon structure. The summation of the respective ionic radii is 2.04 Å for Ta^{+4}-ONN and 2.00 Å for Ta^{+5}-ONN bond lengths, which are of the order of the obtained mean Ta-ONN distances. The difference between the EFGs obtained for Ta^{+4} and Ta^{+5} in the relaxed SCs is still large, albeit reduced in comparison with the difference found for the unrelaxed cases: The V_{ZZ} value at the Ta^{+4} site decreases upon structural relaxation, while V_{ZZ} for Ta^{+5} increases from 10.4×10^{21} V/m^2 (unrelaxed structure) to 12.6×10^{21} V/m^2. The differences in local electronic structure is summarized in Table IV, which shows the partial charges in the Ta muffin-tin sphere, together with the valence contribution to the EFG for both charge states. The main contribution to the EFG comes from the d and p orbitals, while the sd and f contributions are negligible. The main effect of extracting one electron to ionize Ta^{+4} into Ta^{+5} (and the corresponding relaxation of atomic coordinates) is that the p population increases by $+0.03\,e^-$ while the d population decreases by $0.15\,e^-$. As a consequence, the contributions from these orbitals to V_{ZZ} change: For Ta^{+4}, the d contribution is the dominating one ($V_{ZZ}{}^d = 22.1 \times 10^{21}$ V/m^2, $V_{ZZ}{}^p = 4.4 \times 10^{21}$ V/m^2), but when the impurity level is empty (Ta^{+5}) the d contribution drastically decreases to -0.9×10^{21} V/m^2, while the p contribution increases to 13.4×10^{21} V/m^2 and becomes the dominant one.

Finally, after the structural relaxation for the Ta^{+5} charge state the EFG tensor at ZrI and SiI are different (in magnitude and symmetry) from those obtained in pure $ZrSiO_4$, while ZrII and SiII atoms recover the EFGs of the pure system.

The substitution of Zr^{+4} by Ta^{+5} leaves an unpaired electron that, depending on the charge state of the impurity, can lead to a local magnetic moment. This effect has been observed in similar systems [32,33]. Inspired by these results, spin-polarized calculations were performed on the $Zr_{31}TaSi_{32}O_{128}$ system for Ta^{+4} and Ta^{+5} charge states as described above, considering full relaxation of the atomic positions. For the case of Ta^{+5} we did not find a spin-polarized solution (and, therefore, not shown in Tables II–IV). For the case of Ta^{+4}, (L)APW+lo predicts spin polarization with a net magnetic moment of $1.00\,\mu_B$ per unit cell. The major contribution to the magnetic moment comes from the Ta muffin-tin sphere, $0.49\,\mu_B$, and the rest is distributed over the ONN atoms and the interstitial region. The magnetic moment is caused by the

TABLE III. Ta-O bond lengths in Å, and total magnetic moment on Ta in units of μ_B for the different calculations performed.

	$ZrSiO_4$	Unrelaxed $Zr_{31}TaSi_{32}O_{128}$	Relaxed $Zr_{31}TaSi_{32}O_{128}$ Ta^{+4}	Relaxed $Zr_{31}TaSi_{32}O_{128}$ Ta^{+5}	Relaxed and spin-polarized $Zr_{31}TaSi_{32}O_{128}$ Ta^{+4}
d(Ta-ONN1)	2.128	2.128	2.096	2.045	2.109
d(Ta-ONN2)	2.268	2.268	2.195	2.179	2.199
μ^{Ta}	–	–	–	–	0.49

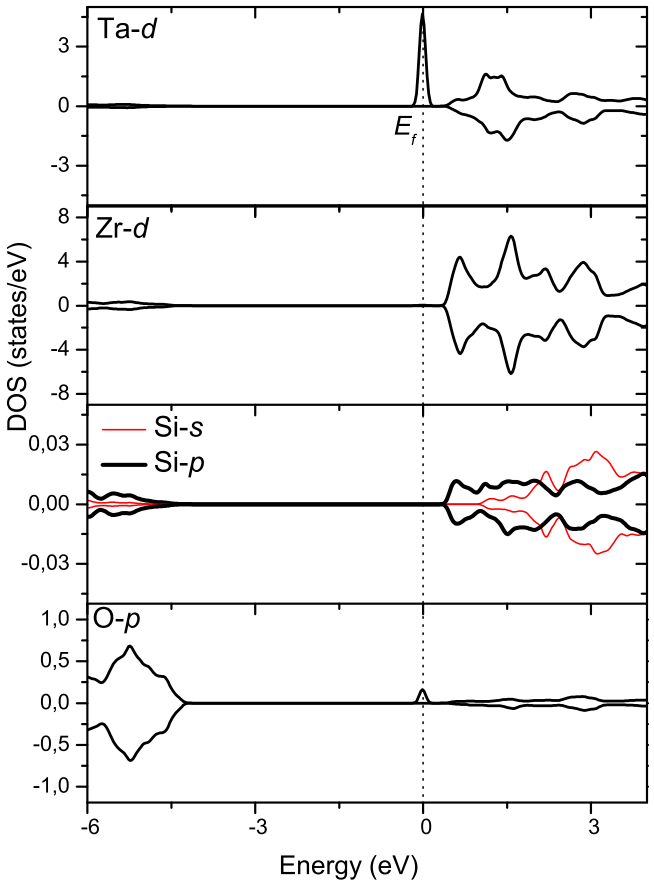

FIG. 5. (Color online) PDOS of Ta-doped $ZrSiO_4$ in the Ta^{+4} charge state with spin-polarized calculation. Energies are referred to as the Fermi level (E_F), which is shown as a vertical dotted line.

polarization of the Ta-5*d* electrons, as can be seen in Fig. 5. The calculated total energies show that the energy difference between the spin-polarized and the nonspin-polarized cases is $\Delta E = E_{sp} - E_{nsp} = -0.09\,\text{eV}$, which is larger than the convergence tolerance. In consequence, the spin-polarized solution is energetically more favorable in the case of Ta^{+4}. The dominant contribution to the EFG at the spin-polarized Ta^{+4} site comes from the d^{up} charge, cf. Table IV. Finally, comparing the EFG for the Ta^{+4} spin-polarized and nonspin-polarized cases (Table IV), the V_{ZZ} values are seen to differ by only 10%.

V. OTHER DEFECTS

Natural (metamictic) zircon contains U and Th as impurities. Although these radioactive nuclei are present in the samples at very low concentrations, the radioactive decay of these elements produce energetic alpha particles that produce some degree of structural disorder. The possible defects that can be created include simple vacancies and interstitials, as well as more extended defect complexes and electron/hole color centers. The latter are difficult to address from the theoretical point of view without experimental information of the defect structure because a large number of possible configurations must be considered. Among the possible structural defects,

TABLE IV. Orbital populations in units of *e*, and *sd*, *p*, *d*, and *f* contributions to the EFG at Ta substitutional sites in Ta-doped $ZrSiO_4$ (in units of $10^{21}\,\text{V/m}^2$) for the different charge states considered as well as the charge state of Ta^{+4}. For all partial contributions $V_{XX} = V_{YY} = -V_{ZZ}/2$.

	Ta^{+4}	Ta^{+5}	Magnetic Ta^{+4}	
	q^{total}	q^{total}	q^{un}	q^{dn}
s	2.05	2.07	1.03	1.02
p	5.70	5.73	2.85	2.85
d	1.26	1.11	0.89	0.40
f	13.96	13.98	6.98	6.98
	Contributions to the EFG			
	Ta^{+4}	Ta^{+5}	Ta^{+4} magnetic q^{up}	Ta^{+4} magnetic q^{dn}
	V_{ZZ}	V_{ZZ}	V_{ZZ}	V_{ZZ}
sd	+0.14	+0.04	0.06	0.08
p	+4.36	+13.35	−0.95	4.22
d	+22.06	−0.88	27.4	−1.57
f	+0.41	+0.12	0.08	0.40
total	+26.97	+12.63	26.59	3.13

the simplest are the oxygen and silicon vacancies, which are also the easiest to model. In the following, the effect of these types of defects on the EFG at Ta sites will be considered. This study requires the examination of the coupling of two types of defects: the Ta impurity probe and the O or Si vacancy itself. Different Ta-Si/O vacancy configurations must be considered in order to determine the equilibrium structures. The study of the energy of each configuration as a function of the impurity-vacancy separation must include the effects of the structural distortions of the cell, and also the charge state of the complex must be examined. As discussed previously, a Ta substituting a Zr atom implies the presence of one extra electron in the Ta vicinity. In a pure ionic model, the O "captures" two electrons from its neighbors. Hence, an O vacancy "leaves" two extra electrons in the cell. In consequence, the combination of the two defects does not seem to be favorable for the reaccommodation of these extra electrons, and within this simple analysis it is expected that the defects will repel each other. On the other hand, the formation of a Si vacancy produces a deficit of four electrons on the O neighbors. As a consequence, this defect can trap the extra electron of the Ta impurity. Thus, for this case we expect that the two defects (Si vacancy and Ta impurity substitutionally replacing Zr) will be as close as possible.

The thermal history and the radiation damage in metamictic samples of zircon are normally not known. Most samples come from volcanic activity. *A priori* it may be expected that a Si-Zr (or Si-Hf) inversion defect could be present in that type of samples before Hf activation, thus leading to a Ta occupying a Si site. We will consider also this type of defect in this section, in order to have the maximum possible Ta configurations to compare with the experimental data. In contrast to natural zircon, *synthesized* samples of $ZrSiO_4$ are not expected to contain defects such as Ta replacing a Si atom.

Finally, the possible formation of domains of silicate due to heavy radiation damage may lead to Ta probes associated with

TABLE V. EFG parameters V_{ZZ} and η for the different defect types and charge states considered. The vacancy location is relative to the Ta site.

System	Vacancy location	Defect charge (e)	V_{ZZ} (10^{21} V/m^2)	η
Zr(Ta)SiO_4 + O vacancy	first neighbor	0	−21.8	0.66
	first neighbor	+3	37.2	0.22
	first neighbor	0	26.5	0.09
	first neighbor	+3	28.2	0.47
Zr(Ta)SiO_4 + Si vacancy	first neighbor	0	15.9	0.25
	first neighbor	–3	−7.4	0.46
	far away	0	12.9	0.06
ZrSi(Ta)O_4	No vacancies	0 (Ta^{+4})	−33.8	0
		+1 (Ta^{+5})	−38.8	0
α-Si(Ta)O_2	No vacancies	0 (Ta^{+4})	18.4	0.02
		+1 (Ta^{+5})	−3.3	0.34

such domains. Additionally, the formation of m-ZrO_2 cannot be excluded. Thus, this work presents EFG calculations for Ta substituting Si in α-SiO_2 in order to further assist the analysis of the experimental results on zircon. For m-ZrO_2, there are many reports of studies using Ta probes that can be compared with zircon experiments to analyze the presence of diluted phases in the zircon samples (see Ref. [29] and references therein). Unfortunately (to the best of the author's knowledge) this is not the case for SiO_2.

A. Oxygen vacancies

In order to study the case of a Ta impurity on a Zr site in the presence of O vacancies, the $2 \times 2 \times 2$ SC previously described was used, removing an oxygen atom and taking into account the structural distortions produced by the vacancy. Thus, the resulting oxygen deficient system is $Zr_{31}TaSi_{32}O_{127}$. The following scenarios are considered: (i) removing an oxygen atom located at 2.13 Å from the Ta site in the unrelaxed structure (ONN1, see Sec. II) and (ii) removing an oxygen atom from the second group of Ta-ONN (ONN2, initially located at 2.27 from Ta). Comparing the total energies of these two cases, it is found that the oxygen vacancy far away from the Ta impurity is more stable than the vacancy near Ta: The total energy of $Zr_{31}TaSi_{32}O_{127}$ with the oxygen vacancy at ONN2 is 0.02 eV lower than the total energy with the oxygen vacancy at ONN1. This result is in line with the previous supposition that the Ta impurity repels the O vacancy, although caution has to be taken because this energy difference is within the convergence limits of the method. Moreover, this energy difference is of the order of kT for 300 K, so a similar number of both types of defects should be expected in real samples. Concerning the EFG tensor, it is seen from Table V that the presence of the oxygen vacancy at site ONN1 produces a large shift in V_{ZZ} and breaks the axial symmetry of the site ($\eta = 0.66$). In contrast, the EFG at the Ta site with a vacancy at ONN2 does not differ significantly from that of the system without vacancies, although the distances from Ta to ONN2 and ONN1 are quite similar.

The argument applied to the charge state of the Ta impurity can also be used for the combined Ta impurity + O vacancy case: The charge compensation in the SC that contains a Ta^{5+} donor impurity and one O vacancy implies the removal of three electrons from the SC, leaving the defect complex with a net charge of $+3e$. Therefore, we calculated the EFG at the Ta site after the removal of three electrons (and compensating the overall charge imbalance with a uniform negative background, as before). For this charge state, our results differ from those of the neutral defect considered above. After full self-consistency and full cell relaxation for both positions of the vacancy, the oxygen vacancy closer to the Ta impurity was found to be more stable than the vacancy further away. The total energy difference is 0.28 eV. The values of V_{ZZ} and η together with the total energy are given in Table V. η is significantly different from zero for both vacancy sites, and for the more stable ONN1 vacancy site the EFG is high: $V_{ZZ} = 37.2 \times 10^{21}$ V/m^2.

B. Si vacancies

In order to analyze the EFG at the Ta site in the case where a Si vacancy has been formed, the $2 \times 2 \times 2$ SC was again used, now removing one Si atom. Again two cases were considered: (i) removing a Si atom closest to the Ta impurity (one of the two SiI atoms at 2.99 Å from Ta) and (ii) removing a Si atom far away from Ta (one of the four SiII atoms at 4.670 Å from Ta). In both cases, extracting one of the 32 Si atoms of the SC represents nearly a 3 at.% vacancy concentration. This value may exceed the Si vacancy concentration in real samples, but it maintains the minimum distance between Si vacancies greater than 11 Å, and then a nearly vanishing vacancy-vacancy interaction is expected.

After relaxing all atomic positions in the presence of the Si vacancy, the total energy and the corresponding EFGs were obtained for both configurations. For the neutral Ta-Si vacancy defect complex, the total energies predict that Si vacancies near Ta are more stable than those further away. The energy difference for the cases considered is 0.60 eV. The presence of the Si vacancy in its more stable configuration reduces the V_{ZZ} value at the Ta site from 27.0×10^{21} V/m^2 for the isolated Ta impurity to 15.9×10^{21} V/m^2 (Ta^{+4} plus a Si vacancy). At the same time, the charge distribution around Ta becomes axially asymmetric, as reflected in the change of the value of η from zero to 0.25. Considering the case of a Si vacancy in the vicinity of Ta, the charge compensation implies the addition of three electrons to the system (of

course, other complex mechanisms for charge compensation may exist). After structural relaxation, the calculation shows a huge change in the V_{ZZ} value to -7.44×10^{21} V/m^2, and the asymmetry parameter is higher than those obtained in the previous case ($\eta = 0.46$).

C. ZrSi(Ta)O_4

The case where Ta replaces a Si atom was also considered within the 2×2×2 SC. As in the previous subsections, the charge state of the impurity was investigated, considering the formal charge states Ta^{+4} and Ta^{+5}. A significant difference with respect to the Zr(Ta)SiO_4 case is that in pure zircon the nearest O atoms are much closer to Si (the Si-O bond lengths are 1.663 Å compared to Zr-O bond lengths of 2.128 Å and 2.268 Å for the Zr site). As a result, replacing a Si atom by a Ta impurity leads to a significant atomic rearrangement: After full relaxation the Ta atom maintains four oxygen atoms as first neighbors but at a distance of 1.84 (1.81) Å for the Ta^{+4} (Ta^{+5}) charge state, i.e., for ZrSi(Ta)O_4 there is an increase of about 10% in the Ta-O bond length, while for Zr(Ta)SiO_4 there is a contraction of the Ta-O bond length, as discussed before. The obtained EFGs are summarized in Table V. The Si site has axial symmetry, so $\eta = 0$.

D. α-Si(Ta)O_2

To calculate the EFG at a Ta impurity substituting a Si atom in α-SiO_2, we have used the recent experimental structural data reported in Ref. [36]. The lattice constants of the single cell are $a = 4.9019$ Å, $c = 5.3988$ Å, the space group is $P3_121$, and the internal coordinates are $x = 0.4673$ for Si and $x = 0.4130$, $y = 0.2711$, and $z = 0.2172$ for O. Then, we built a 2×2×2 SC that contains 72 atoms and replaced one Si by a Ta atom (an ordered system $Si_{23}TaO_{48}$, Ta impurity concentration 4.2 at. %). The minimum Ta-Ta separation due to the periodic boundary conditions is 9.92 Å. As in the case of Ta-doped zircon, a careful study of the basis set and the k-point sampling was performed. This study showed that for $R_{mt}K_{\max} = 6$ and 100 k-points in the BZ (38 in the IBZ), the EFG components and bond lengths are very well converged. The Ta, Si, and O muffin-tin radii used were 0.81 Å, 0.77 Å, and 0.77 Å, respectively. In the following, we will present the main results obtained in Ta-doped α-SiO_2, with focus on a discussion of the EFG. A more detailed study will be presented in a forthcoming paper.

Similar to the case of Ta substituting Zr in zircon, we also analyzed different charge states in order to study the effects of charge compensation when the Ta^{+5} impurity probe replaces Si^{+4}. In the following, we will use the same nomenclature as before (Ta^{+4} and Ta^{+5}) to describe both charge states. In Fig. 6, the partial DOS for Ta, Si, and O are shown. In the left panel, it can be seen that, as in the case of zircon, the Ta^{+4} generates a sharp donor impurity level at the Fermi level. These states have Ta-d character and are shifted toward the conduction band when the extra electron is removed (Ta^{+5} charge state). The predicted EFG at the Ta^{+4} site resulted in $V_{zz} = 18.4 \times 10^{21}$ V/m^2 and $V_{ZZ} = -3.3 \times 10^{21}$ V/m2 for the site Ta^{+5} (Table V). This huge difference in the EFGs for both charge states is larger than the TDPAC resolution, so experimental data should be very valuable in determining the charge state of the Ta probe in α-SiO_2 and in determining a possible coexistence of different charge states at a given temperature for this particular host-impurity system.

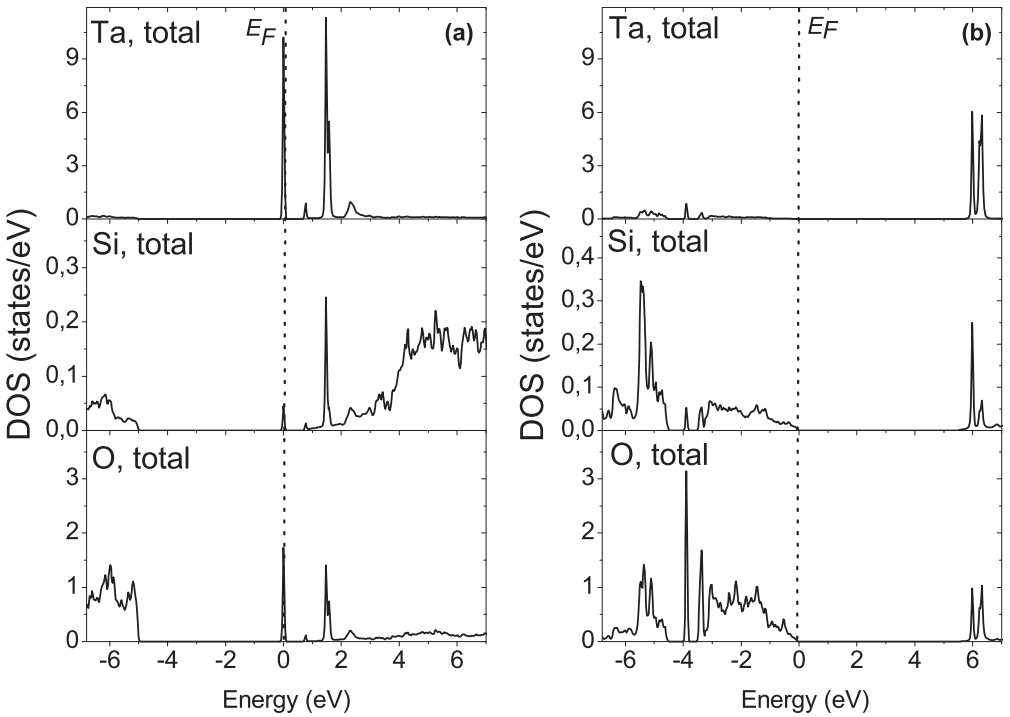

FIG. 6. PDOS of Ta-doped α-SiO_2 in the Ta^{+4} (a) and Ta^{+5} (b) charge states. Energies are referred to as the Fermi level (E_F), which is shown as a vertical dotted line.

TABLE VI. Summary of experimental quadrupole interactions for Ta in zircon and *ab initio*-based assignments of the hyperfine interactions (NQI) experimentally observed at ^{181}Ta probes in $ZrSiO_4$ samples to crystallographic sites.

Paper	Sample	Fraction (%)	$V_{ZZ}{}^{exp}$ (10^{21} V/m^2)	η	δ (%)	NQI label	Site assignment
Jaeger *et al.* 1997 [10]	metamictic	100	10.96	0	4–12	NQI1	Ta^{+5} replacing Zr
Rivas *et al.* [11]	synthetic	100	11.31	0.21	10	NQI1	Ta^{+5} replacing Zr
Jaeger and McBride [12]	synthetic	90	11.50	0.13	3	NQI1	
		40–50	not determined	–	–	NQI2	Ta^{+4} replacing Zr, spin-polarized
		10	14.04	0.335	3	NQI3	Ta^{+5} replacing Zr in *m*-ZrO2
Rendtorff *et al.* [13]	synthetic	50	11.53	0	3	NQI1	Ta^{+5} replacing Zr
		50	9.52	0.74	15	NQI4	–

VI. COMPARISON WITH TDPAC EXPERIMENTS

Several measurements of the EFG in $ZrSiO_4$ samples by means of TDPAC spectroscopy using ^{181}Ta as probes were reported in the literature. The corresponding results are summarized in Table VI. Jaeger *et al.* [10] performed measurements on metamictic samples and found one NQI characterized by $V_{ZZ} = 10.96 \times 10^{21}$ V/m^2 and $\eta = 0.00$. The authors assigned this NQI to Ta, substitutionally replacing Zr in the $ZrSiO_4$ structure. This NQI is characterized by a frequency distribution width (δ) of 12%, evidence of a nonnegligible host disorder in the vicinity of the probe atoms. This frequency distribution has been related to radiation damage produced by α particles originating from the decays of Th and U impurities in the sample. After thermal treatments, δ was reduced to 4%. Subsequently, Rivas *et al.* [11] studied synthetic samples of $ZrSiO_4$. They also found a unique NQI characterized by $V_{ZZ} = 11.31 \times 10^{21}$ V/m^2, $\eta = 0.21$, and $\delta = 10\%$. Besides the similar hyperfine parameters obtained, two points deserve attention. First, the obtained η value does not correspond to the expected axial symmetry of the Zr site. Second, the synthetic samples are not supposed to have radiation damage, whereby the δ parameter would be expected to be lower.

Jaeger and McBride [12] performed new measurements on zircon, but this time the TDPAC experiments were performed on synthetic samples. The new results are more complex than the previous ones: The authors determined three NQIs. One of the NQIs (90% fraction, $V_{ZZ} = 11.50 \times 10^{21}$ V/m^2) was assigned to the regular Zr site but had a small deviation from axial symmetry ($\eta = 0.13$) and $\delta = 3\%$ at room temperature. The second NQI, with a relative fraction of 10%, $V_{ZZ} = 14.05_4 \times 10^{21}$ V/m^2, $\eta = 0.335_5$, and $\delta = 2_1\%$ was assigned to Ta in the spurious *m*-ZrO_2 phase present in the samples. Unfortunately, no x-ray diffraction experiments were done to confirm the presence of *m*-ZrO_2 in the samples. Additionally, the authors performed TDPAC experiments as a function of temperature and observed an unexpected change in the experimental spectra (a reduction in the time-zero anisotropy A_2 at temperatures below 600 °C). The authors explained this reduction of A_2 as arising from an electronic defect of some sort, which at sufficiently high temperature is removed. This reduction of the time-zero anisotropy can be associated to the presence of a hyperfine interaction characterized by a high V_{ZZ} value that cannot be resolved, and, in consequence, it is not possible to determine the V_{ZZ} and η values. They estimated that 40–50% of the probe atoms were "exposed" to this defect. Interestingly, a similar effect has been observed in TDPAC experiments performed in ^{181}Ta-doped *m*-ZrO_2 and *m*-HfO_2, explained in Refs. [32,33].

Finally, in a recent paper, Rendtorff *et al.* [13] found two different NQIs in synthetic zircon samples. The interactions were characterized by $V_{ZZ} = 11.53 \times 10^{21}$ V/m^2, $\eta = 0.00$, and $\delta = 3\%$; and $V_{ZZ} = 9.52 \times 10^{21}$ V/m^2, $\eta = 0.74$, and $\delta = 15\%$. Both interactions have initially the same relative fraction, but after thermal treatments the relative fraction of the first interaction grows up to 75%.

Summarizing the experimental results reported in the literature, we may separate the different NQIs into four groups (see Table VI): a NQI characterized by a value of V_{ZZ} in the range $10.96 - 11.53 \times 10^{21}$ V/m^2 and a low η value (0.00–0.21). This interaction (hereafter named NQI1) was observed in all the experiments and in all cases has a low frequency distribution and a large relative fraction and was associated to Ta at the regular Zr site in $ZrSiO_4$. According to our theoretical results, NQI1 is compatible with Ta probes substitutionally located at the Zr sites of $ZrSiO_4$ in the charge state Ta^{+5} (impurity donor level empty). The interaction observed by Jaeger and McBride [12] in TDPAC experiments in synthetic zircon characterized by a high V_{ZZ} value (NQI2) cannot be unambiguously fitted. There are four scenarios considered in our calculations with high V_{ZZ} values:

(i) Ta replacing Zr in the charge state Ta^{+4} [donor impurity level partially occupied ($V_{ZZ} = 27.0 \times 10^{21}$ V/m^2 and $\eta = 0.00$)].

(ii) Ta replacing Zr in the same Ta^{+4} charge state but with a local magnetic splitting ($V_{ZZ} = 29.7 \times 10^{21}$ V/m^2 and $\eta = 0.00$).

Comparing total energies for the (i) and (ii) cases the lowest energy solution corresponds to the spin polarized case.

(iii) Ta with a nearby oxygen vacancy removing three electrons from the cell. Considering that the synthetic zircon sample underwent different thermal treatments and the fact that the fraction of probes that "felt" this NQI depends in a reversible way on the temperature, this scenario seems unlikely.

(iv) Ta replacing Si for both charge states ($V_{ZZ} = -33.8 \times 10^{21}$ V/m^2; $\eta = 0$ and $V_{ZZ} = -38.8 \times 10^{21}$ V/m^2; $\eta = 0$). Due to the fact that the samples employed are synthetic, and in view of the method used for the introduction of the TDPAC probe (neutron irradiation of naturally occurring ^{180}Hf to obtain ^{181}Hf), it is not expected that the probes ^{181}Hf $\rightarrow$ ^{181}Ta

populate Si sites (on the other hand, this situation could be expected, for example, in the case of ionic implantation of the probes).

In conclusion, and similar to the previous findings of Ta-doped m-ZrO_2 and m-HfO_2, our theoretical results indicate that two different charge states may coexist in Ta-doped $ZrSiO_4$: Ta^{+4} and Ta^{+5}. This conclusion is fully compatible with the results obtained by Jaeger and McBride [12]. The population of NQI2 diminishes as a function of the temperature. This behavior could be associated with the thermal activation of the ionization of the impurity level induced by the Ta impurity. At room temperature, 40–50% of the probes should be initially in the Ta^{+4} charge state, while at high temperatures the fraction of probes in the Ta^{+4} state should diminish, favoring the Ta^{+5} charge state. It would be interesting to perform new TDPAC experiments as a function of temperature but now assuming that NQI2 have a combined electric and magnetic nature.

The interaction observed by Jaeger and McBride [12] in synthetic samples, characterized by $V_{ZZ} = 14.05_4 \times 10^{21}\,\mathrm{V/m^2}$, $\eta = 0.335_5$ (NQI3), can be associated (based on previous TDPAC experiments and *ab initio* calculations, Ref. [33]) to Ta probes replacing Zr in a spurious m-ZrO_2 phase.

The NQI characterized by $V_{ZZ} = 9.52 \times 10^{21}\,\mathrm{V/m^2}$ and $\eta = 0.74$ was observed only in the paper of Rendtorff *et al.* (NQI4) [13]. This interaction is not fully compatible with any of the configurations previously discussed here. The only NQI found in this paper with comparable V_{ZZ} and η values is that corresponding to the Si vacancy combined with Ta in a Zr regular site, including three electrons to the cell ($V_{ZZ} = -7.4 \times 10^{21}\,\mathrm{V/m^2}$ and $\eta = 0.46$), but comparing the experimental and predicted values they differ by about 25%, which is large enough to be conclusive. The population of NQI4 is reduced by a factor of two after annealing, so this interaction may be related with some other kind of defect or spurious phase produced during the sample preparation.

Finally, the predicted V_{ZZ} and η values for Ta in α-SiO_2 are not coincident with any of the experimentally observed NQI in $ZrSiO_4$ samples. This disagreement discards the possibility that one of the observed NQI correspond to Ta in α-SiO_2.

VII. CONCLUSIONS

Pure and Ta-doped zircon were studied by means of *ab initio* calculations within the density functional theory, with special emphasis on the analysis of the EFG at the Zr and Ta site. The pure system $ZrSiO_4$ was studied as a test case in order to validate the model employed to reproduce the EFG values measured by NMR at the Zr site. Also, the band gap was analyzed in terms of the modified Becke-Johnson correction to the LDA. The Ta-doped system was simulated by means of the SC approximation using a 192-atom unit cell. Several defects including different charge states of the Ta atom, both without and with associated O and Si vacancies, were studied and compared with the experimental data. As a result, we conclude that our results are compatible with Ta acting in the samples with two different charge states when replacing Zr^{+4}: Ta^{+5} and Ta^{+4}. The first one corresponds to the quadrupole interaction commonly associated with the regular Ta site in zircon, while Ta^{+4} is characterized by an axially symmetric EFG tensor with a high value of V_{ZZ}. This high V_{ZZ} is difficult to observe in TDPAC experiments but may be responsible for the drop in the time-zero anisotropy as a function of temperature observed in the experiments of Jaeger and McBride [12]. The present paper also predicts that this last interaction should be a combined magnetic plus quadrupolar electric interaction, a result based on the total energy calculations of the spin-polarized and nonspin-polarized cases. Also, we analyzed the case of α-$Si(Ta)O_2$ as a possible source of the unexplained NQIs detected. The configurations analyzed lead to V_{ZZ} values, which are not compatible with any of the measured values.

ACKNOWLEDGMENTS

This paper was partially supported by the Consejo Nacional de Investigaciones Científicas y Técnicas (CONICET) under Project No. PIP 0002 and UNNOBA (Project SIB082). This research made use of the HP-Parallel-Computing Bose Cluster, the computational facilities of the Physics of Impurities in Condensed Matter group, at the Instituto de Física La Plata (IFLP) and the Departamento de Física (UNLP) and the CSC-AA Computing Centre, Aarhus University, Aarhus, Denmark.

[1] J. P. Crocombette, Phys. Chem. Miner. **27**, 138 (1999).
[2] R. C. Ewing, W. Lutze, and W. J. Weber, J. Mater. Res. **10**, 243 (1995).
[3] G. D. Wilk, R. M. Wallace, and J. M. Anthony, J. Appl. Phys. **89**, 5243 (2001); R. Puthenkovilakam, E. A. Carter, and J. P. Chang, Phys. Rev. B **69**, 155329 (2004).
[4] R. Terki, G. Bertrand, and H. Aourag, Microelectron. Eng. **81**, 514 (2005).
[5] E. Balan, F. Mauri, C. Pickard, I. Farnan, and G. Salas, Am. Mineral. **88**, 1769 (2003); H. D. Holland and D. Gottfried, Acta Crystallogr. **8**, 291 (1955).
[6] E. K. H. Salje, J. Chrosch, and R. C. Ewing, Am. Mineral. **84**, 1107 (1999); S. Ríos, E. K. H. Salje, M. Zhang, and R. C. Ewing, J. Phys.: Condens. Matter **12**, 2401 (2000).
[7] T. Murakami, B. C. Chakoumakos, R. C. Ewing, G. R. Lumpkin, and W. J. Weber, Am. Mineral. **76**, 1510 (1991); W. J. Weber, R. C. Ewing, and L. M. Wang, J. Mater. Res. **9**, 688 (1994).
[8] C. Y. Chain, S. Ferrari, L. C. Damonte, J. A. Martínez, and A. F. Pasquevich, J. Alloys Compd. **536S**, S50 (2012); C. Y. Chain, L. C. Damonte, S. Ferrari, E. Muñoz, C. Rodríguez Torres, and A. F. Pasquevich, *ibid.* **495**, 527 (2010); A. Vasquez, J. D. Rogers, A. Maciel, and E. R. Fraga, Rev. Bras. Fis. **3**, 311 (1973); L. Rubio-Puzzo, M. C. Caracoche, M. Cervera, P. C. Rivas, A. M. Ferrari, and F. Bondioli, J. Solid State Chem. **150**, 14 (2000).
[9] T. J. Bastow, J. Phys.: Condens. Matter **2**, 6327 (1990).
[10] H. Jaeger, L. Abu-Raddad, and D. Wick, Appl. Radiat. Isot. **48**, 1083 (1997).

[11] P. C. Rivas, P. C. Ferrari, and A. M. Bondioli, Solid State Chem. **150**, 14 (2000).
[12] H. Jaeger and S. P. McBride, Hyperfine Interact. **177**, 51 (2007).
[13] N. M. Rendtorff, M. S. Conconi, E. F. Aglietti, C. Y. Chain, A. F. Pasquevich, P. C. Rivas, J. A. Martínez, and M. C. Caracoche, Hyperfine Interact. **198**, 219 (2010).
[14] K. Robinson, G. V. Gibbs, and P. H. Ribbe, Am. Mineral. **56**, 782 (1971).
[15] B. A. Kolesov, C. A. Geiger, and T. Armbruster, Eur. J. Mineral. **13**, 939 (2001).
[16] See, e.g., G. Schatz and A. Weidinger, *Nuclear Condensed Matter Physics—Nuclear Methods and Applications* (Wiley, Chichester, 1996), pp. 21–100; E. N. Kaufmann and R. J. Vianden, Rev. Mod. Phys. **51**, 161 (1979); H. Frauenfelder and R. M. Steffen, in *Alpha-, Beta-, and Gamma-Ray Spectroscopy*, edited by K. Siegbahn (North Holland, Amsterdam, 1966), Vol. 2, pp. 997–1262.
[17] K. Schwarz, C. Ambrosch-Draxl, and P. Blaha, Phys. Rev. B **42**, 2051 (1990).
[18] T. Butz and A. Lerf, Phys. Lett. A **97**, 217 (1983).
[19] S. Buttgenbach, in *Hyperfine Structure in 4d- and 5d-Shell Atoms*, Springer Tracts in Modern Physics, Vol. 96 (Springer, Berlin, 1982), pp. 78–86.
[20] E. Sjöstedt, L. Nordström, and D. J. Singh, Solid State Commun. **114**, 15 (2000); G. K. H. Madsen, P. Blaha, K. Schwarz, E. Sjöstedt, and L. Nordström, Phys. Rev. B **64**, 195134 (2001); S. Cottenier, *Density Functional Theory and the Family of (L)APW-Methods: A Step-by-Step Introduction* (KU Leuven, Belgium, 2002), http://www.wien2k.at/reg_user/textbooks
[21] P. Blaha, K. Schwarz, G. K. H. Madsen, D. Kvasnicka, and J. Luitz, WIEN2k, in *An Augmented Plane Wave Plus Local Orbitals Program for Calculating Crystal Properties*, edited by K. Schwarz (Technical Universität Wien, Austria, 1999).
[22] R. E. Alonso, L. A. Errico, E. L. Peltzery Blanća, A. López-García, A. Svane, and N. E. Christensen, Phys. Rev. B **78**, 165206 (2008).
[23] G. Fadda, L. Colombo, and G. Zanzotto, Phys. Rev. B **79**, 214102 (2009).
[24] P. E. Blöchl, O. Jepsen, and O. K. Andersen, Phys. Rev. B **49**, 16223 (1994).
[25] J. P. Perdew and Y. Wang, Phys. Rev. B **45**, 13244 (1992).
[26] J. P. Perdew, A. Ruzsinszky, G. I. Csonka, O. A. Vydrov, G. E. Scuseria, L. A. Constantin, X. Zhou, and K. Burke, Phys. Rev. Lett. **100**, 136406 (2008).
[27] V. Kellö, P. Pyykkö, A. J. Sadlej, P. Schwerdtfeger, and J. Thyssen, Chem. Phys. Lett. **318**, 222 (2000).
[28] S. L. Votyakov, I. P. Ivanov, A. A. Krasnobayev, V. Y. Krokhalev, and V. S. Korzhinskaya, Neorganicheskie Materialy **22**, 281 (1986); A. Krasnobayev, S. Votyakov, and V. Krohalev, *Spectroscopy of Zircons (Properties and Geological Application)* (Nauka, Moscow, 1988); F. Cesbron, D. Ohnenstetter, P. Blanc, O. Rouer, and M. C. Sichere, C. R. Acad. Sci. Paris **316**, 1231 (1993); L. Nasdala, M. Zhang, U. Kempe, G. Panczer, M. Gaft, M. Andrut, and M. Plötze, Rev. Mineral. Geochem., January v. **53**, 427 (2003).
[29] A. Kawamoto, K. Cho, P. Griffin, and R. Dutton, J. Appl. Phys. **90**, 1333 (2001).
[30] J. P. Perdew and A. Zunger, Phys. Rev. B **23**, 5048 (1981).
[31] F. Tran and P. Blaha, Phys. Rev. Lett. **102**, 226401 (2009); A. D. Becke and E. R. Johnson, J. Chem. Phys. **124**, 221101 (2006).
[32] M. A. Taylor, R. E. Alonso, L. A. Errico, A. López-García, P. de la Presa, A. Svane, and N. E. Christensen, Phys. Rev. B **82**, 165203 (2010).
[33] M. A. Taylor, R. E. Alonso, L. A. Errico, A. López-García, P. de la Presa, A. Svane, and N. E. Christensen, Phys. Rev. B **85**, 155202 (2012).
[34] S. H. Choh, H. Won Shin, II-Woo Park, H. Ju, J. Hyun Kim, and H. Jin Kim, J. Korean Magn. Reson. Soc. **7**, 16 (2003); G. Belford, R. A. Bernheim, and H. S. Gutowsky, J. Chem. Phys. **35**, 1032 (1961); N. Subramani, J. Mol. Struct. **1**, 369 (1989); T. Butz, Z. Naturforsch. A **57**, 518 (2002).
[35] R. D. Shanon, Acta Crystallogr. Sect. A **32**, 751 (1976).
[36] M. G. Tucker, D. A. Keen, and M. T. Dove, Mineral. Mag. **65**, 489 (2001).